The Astrophysical Journal, 925:8 (7pp), 2022 January 20 https://doi.org/10.3847/1538-4357/ac35cb

Results From an Einstein@Home Search for Continuous Gravitational Waves From G347.3 at Low Frequencies in LIGO O2 Data

J. Ming[1,2], M. A. Papa[1,2,3], H.-B. Eggenstein[1,2], B. Machenschalk[1,2], B. Steltner[1,2], R. Prix[1,2], B. Allen[1,2,3], and O. Behnke[1,2]

[1] Max Planck Institute for Gravitational Physics (Albert Einstein Institute), Callinstrasse 38, D-30167 Hannover, Germany; jing.ming@aei.mpg.de, maria.alessandra.papa@aei.mpg.de
[2] Leibniz Universität Hannover, D-30167 Hannover, Germany
[3] University of Wisconsin Milwaukee, 3135 N Maryland Ave, Milwaukee, WI 53211, USA
Received 2021 August 16; revised 2021 October 18; accepted 2021 November 1; published 2022 January 20

Abstract

We present results of a search for periodic gravitational wave signals with frequencies between 20 and 400 Hz from the neutron star in the supernova remnant G347.3-0.5 using LIGO O2 public data. The search is deployed on the volunteer computing project Einstein@Home, with thousands of participants donating compute cycles to make this endeavour possible. We find no significant signal candidate and set the most constraining upper limits to date on the amplitude of gravitational wave signals from the target, corresponding to deformations below 10^{-6} in a large part of the band. At the frequency of best strain sensitivity, near 166 Hz, we set 90% confidence upper limits on the gravitational wave intrinsic amplitude of $h_0^{90\%} \approx 7.0 \times 10^{-26}$. Over most of the frequency range our upper limits are a factor of 20 smaller than the indirect age-based upper limit.

Unified Astronomy Thesaurus concepts: Gravitational wave astronomy (675); Neutron stars (1108); Supernova remnants (1667)

1. Introduction

Continuous gravitational waves (CWs) are among the gravitational wave signals that have not yet been detected. Fast spinning neutron stars with non-axisymmetric deformations or with unstable *r*-modes are expected to emit continuous waves that lie in the high-sensitivity frequency range of ground-based interferometers (Owen et al. 1998; Owen 2010; Lasky 2015).

Although the expected waveforms are fairly simple, the search for continuous wave signals is very challenging due to their extreme weakness. A signal-to-noise ratio (S/N) is accumulated by integrating the signal over many months, and this increases our ability to resolve different waveforms. This also means that if the signal waveform is not a priori known, many different waveforms must be searched for, and the computing cost increases very significantly. In fact, when searching a broad range of waveforms, the sensitivity of continuous wave searches is usually limited by the computing power.

Since the Advanced LIGO (Abbott et al. 2015) detectors began observations, various continuous waves searches have been carried out. Among them, the searches for continuous waves from known pulsars, with known spin frequency and frequency evolution, are the most sensitive and computationally inexpensive (Abbott et al. 2019a, 2021a; Ashok et al. 2021). At the other extreme, there are the all-sky surveys with no prior information of frequency and sky location (Dergachev & Papa 2021a, 2020, 2021b; Steltner et al. 2021b; Abbott et al. 2019b, 2021b, 2021c; Covas & Sintes 2020). In between, the directed searches target locations in the sky that are known or suspected to harbor a neutron star, although a pulsation shape has generally not been observed. Searches of this type include the Galactic Center (Dergachev et al. 2019; Piccinni et al. 2020), young supernova remnants (SNRs; Ming et al. 2019; Abbott et al. 2019c; Millhouse et al. 2020; Lindblom & Owen 2020; Papa et al. 2020; Abbott et al. 2021d), glitching pulsars (Fesik & Papa 2020; Abbott et al. 2021e), and low-mass X-ray binaries such as Scorpius X-1 (Zhang et al. 2021).

Young neutron stars are good continuous wave candidates: an indirect upper limit can be placed on the continuous gravitational wave strength that is proportional to $1/\sqrt{\tau}$, with τ being the age of the neutron star (Wette et al. 2008; Zhu et al. 2016). Fifteen young SNRs have been identified in our Galaxy that could host a young neutron star and potentially be promising targets. Recent searches probe emission from *all* of these over a broad range of waveforms (Lindblom & Owen 2020; Abbott et al. 2021d).

An alternative approach is to identify the most promising targets and concentrate the search efforts on these. In Ming et al. (2016), we propose an optimization scheme to decide how to spend the computing budget in such a way to maximize the detection probability. With a computing budget of a few months on the Einstein@Home volunteer computing project (Einstein@Home 2019), the indication is to search for emission from the neutron star in the SNRs Vela Jr. (G266.2-1.2), Cassiopeia A (G111.7-2.1), and G347.3 (G347.3-0.5). We carried out searches using O1 data, and O2 data for follow-ups, and set the most constraining upper limits on gravitational wave emission from these sources with those data (Ming et al. 2019; Papa et al. 2020).

In Papa et al. (2020), we also found a subthreshold candidate at around 369 Hz. Gravitational wave follow-ups were not completely conclusive and we found no evidence of pulsations from searches of archival X-ray data to validate this candidate, but the X-ray searches had limited sensitivity. Abbott et al. (2021d) did not find this candidate in the first half of O3 data; however the sensitivity of Abbott et al. (2021d) is lower than that of our original search. We thus prioritize a deep search for

G347.3 in the O2 data below 400 Hz. This paper presents results from such a search.

The paper is organized as follows. In Section 2 we review the astrophysical target and the model gravitational waveform. After a brief description of the data in Section 3, in Section 4 we describe the search. The results follow in Section 5, where we explain how the $h_0^{90\%}$ intrinsic continuous gravitational wave amplitude upper limits are derived. These are also recast as upper limits on the star's ellipticity and *r*-mode saturation. We conclude with a discussion of the results, comparing and contrasting with existing literature in Section 6.

2. The Target

2.1. G347.3-0.5

The SNR G347.3 is suggested to be the remnant of the AD393 "guest star" (Wang et al. 1997). We therefore assume an age of 1600 years, although this estimate is not completely uncontroversial (Fesen et al. 2012). Using XMM data, Cassam-Chenaï et al. (2004) estimate its distance to be around 1.3 kpc. The position of the central compact object in the G347.3 SNR is given with subarcsecond accuracy in Mignani et al. (2008), based on Chandra data. Among the SNRs in our galaxy, G347.3 is one of the most interesting directed search targets because of its relatively young age and close distance (Ming et al. 2016).

In the deep CW search for G347.3 in O1 data (Papa et al. 2020), we find an interesting candidate at around 369 Hz. The spindown energy loss from the candidate parameters yields an unusually high value, 1.6×10^{40} erg s^{-1}, which exceeds the most energetic Crab pulsar's $\dot{E} = 4.6 \times 10^{38}$ erg s^{-1} and J0537-6910's $\dot{E} = 4.9 \times 10^{38}$ erg s^{-1}.

2.2. The Signal

We assume a standard IT2 continuous gravitational wave signal (Dergachev & Papa 2021b) produced by asymmetric rotating neutron stars that, in the detector data, has a form (Jaranowski et al. 1998):

$$h(t) = F_+(t)h_+(t) + F_\times(t)h_\times(t), \tag{1}$$

where $F_+(t)$ and $F_\times(t)$ are the antenna pattern functions of the detector for the two gravitational wave polarizations "+" and "×". They depend on the sky position of the source (defined by the R.A. and decl.), and the orientation ψ of the wave frame with respect to the detector frame. $F_+(t)$ and $F_\times(t)$ are periodic time functions with a period of one sidereal day, because the detector rotates with the Earth.

The phase $\Phi(t)$ of the signal at the solar system barycenter (SSB) frame has the form:

$$\Phi(\tau_{\rm SSB}) = \Phi_0 + 2\pi[f(\tau_{\rm SSB} - \tau_{0\rm SSB}) + \frac{1}{2}\dot{f}(\tau_{\rm SSB} - \tau_{0\rm SSB})^2 + \frac{1}{6}\ddot{f}(\tau_{\rm SSB} - \tau_{0\rm SSB})^3], \tag{2}$$

where f is the signal frequency and $\tau_{\rm SSB}$ is the arrival time of the GW front at the SSB frame.

3. The Data

The LIGO O2 public data (LIGO 2019; Abbott et al. 2021f) are used in this search. The data are from the two observatories in the USA, one in Hanford (Washington) and the other in Livingston (Louisiana). The data used in this search are between GPS time 1167983370 (2017 Jan 09) and 1187731774 (2017 Aug 25). Short Fourier transforms (SFTs) of data segments 1800 seconds long (Allen & Mendell 2004) are created as is customary for Einstein@Home searches.

Calibration lines, the mains power lines, and some other spurious noise due to the LIGO laser beam jitter are removed in the publicly released O2 data (Davis et al. 2019). Additionally we remove loud short-duration glitches with the gating procedure described in Steltner et al. (2021a) and substitute Gaussian noise in the frequency domain in disturbed bins. This is a standard procedure in Einstein@Home searches.

4. The Search

We use a "stack-slide" type of search based on the GCT (Global correlation transform) method (Pletsch 2008, 2010; Pletsch & Allen 2009). The data are partitioned in $N_{\rm seg}$ segments and each segment spans a duration $T_{\rm coh}$. The data of both detectors from each segment i are searched with a maximum likelihood coherent method to construct the detection statistic, $\mathcal{F}$-statistic (Jaranowski et al. 1998; Cutler & Schutz 2005). The statistics $\mathcal{F}_i$ from the coherent searches of the different segments are summed, and the value of the core detection statistic $\overline{\mathcal{F}}$ is obtained:

$$\overline{\mathcal{F}} := \frac{1}{N_{\rm seg}}\sum_{i=1}^{N_{\rm seg}}\mathcal{F}_i. \tag{3}$$

In Gaussian noise $N_{\rm seg} \times 2\overline{\mathcal{F}}$ follows a chi-squared distribution with $4N_{\rm seg}$ degrees of freedom, and a noncentrality parameter ρ^2. If a signal is present, ρ^2 is proportional to $\frac{h_0^2 T_{\rm obs}}{S_h}$, where S_h is the strain power spectral density of the noise at the frequency of the signal, and h_0 is the signal intrinsic amplitude at Earth (Jaranowski et al. 1998).

Small portions of the data exist that are not perfectly Gaussian, and despite the removal of many spectral lines of instrumental and environmental origin, some coherent disturbances persist (Covas et al. 2018). The $\overline{\mathcal{F}}$ can be affected by these coherent disturbances and present increased values. In order to mitigate these occurrences, a line robust detection statistic $\hat{\beta}_{\rm S/GLtL}$ (Keitel et al. 2014; Keitel 2016) is computed. This statistic is the log of a Bayesian odds ratio that tests the signal hypothesis (S) versus an extended noise hypothesis. The "GLtL" noise model of this statistic consists of Gaussian noise (G) or coherent single-detector signals that are always-ON (lines, L) or transient lines (tL).

The Einstein@Home results from this search are ranked according to $\hat{\beta}_{\rm S/GLtL}$, such that the top list contains fewer candidates produced by coherent disturbances.

The search setup, i.e., the coherent baseline $T_{\rm coh}$, the template grid spacings, and the search ranges are all derived from the optimization procedure.

We search for signal waveforms with frequency and frequency derivatives as follows:

$$\begin{cases} 20\ \text{Hz} \leqslant f \leqslant 400\ \text{Hz} \\ -f/\tau \leqslant \dot{f} \leqslant 0\ \text{Hz/s} \\ 0\ \text{Hz/s}^2 \leqslant \ddot{f} \leqslant 7\,|\dot{f}|^2_{\rm max}/f = 7f/\tau^2, \end{cases} \tag{4}$$

Table 1
Spacings on the Signal Parameters Used for the Templates in the Search

Search Setup					
$T_{\rm coh} = 1080$ hr	$N_{\rm seg} = 5$	$\delta f = 1.3 \times 10^{-7}$ Hz	$\delta \dot{f} = 1.5 \times 10^{-14}$ Hz s^{-1}	$\delta \ddot{f} = 1.2 \times 10^{-20}$ Hz s^{-2}	$T_{\rm ref} = 1177858472.0$[a]

Note.
[a] Barycentric Dynamical Time in GPS seconds.

where $\tau = 1600$ years. The ranges for $\dot{f}$ and $\ddot{f}$ correspond to different breaking index n values, namely 2 and 7. In the $\dot{f}$ equation, $n = 2$ is used to encompass the broadest range of $\dot{f}$ values. In the $\ddot{f}$ equation, $n = 7$ is used to encompass all astrophysical scenarios including the phase evolution purely due to gravitational wave emission ($n = 5$) and r-mode oscillations ($n = 7$). At 400 Hz, the $\dot{f}$ extends down to -8.0×10^{-9} Hz s^{-1} and the $\ddot{f}$ range up to 1.1×10^{-18} Hz s^{-2}.

The grid spacings in frequency and spindowns are constant over these search ranges and are given in Table 1. The number of searched templates per 1 Hz band increases as the frequency increases, as Equation (4) shows. Figure 1 shows the number of templates searched in 1 Hz bands as a function of frequency.

The search is performed on the Einstein@Home volunteer computing project. Einstein@Home is built on the BOINC (Berkeley Open Infrastructure for Network Computing) architecture (Anderson 2004; Anderson et al. 2006), which uses the idle time on volunteer computers to tackle scientific problems such as this that require large amounts of computing power.

Overall we search $\approx 5.1 \times 10^{16}$ templates, utilizing Einstein@Home for several weeks. The workload is split in work units, sized to keep the average volunteer host busy for 8 hours. The whole search task is split into about 2.5 million work units. Only information from the most promising 10,000 results from each work unit is communicated back to the central Einstein@Home server.

5. Results

After the Einstein@Home server has received all search results, the post-processing begins. In total we have 2.5 million work units times 10,000 results returned per work unit $\approx 2.5 \times 10^{10}$ search results. Each result is identified by the template waveform parameters $(f, \dot{f}, \ddot{f})$ and by the detection statistics values.

With a parameter-space clustering procedure we identify the most interesting results (Singh et al. 2017; Beheshtipour & Papa 2020, 2021; Steltner et al. 2021b). We refer to these as "candidates".

We consider the top 1 million candidates, corresponding to a detection statistic threshold $\hat{\beta}_{\rm S/GLtLr} = 1.948$. The subscript "$r$" refers to a recomputation of the detection statistic performed on all top-list candidates. This recomputation is a typical step in a semicoherent search, where the detection statistic is an approximation of the exact value for any given template. The recomputation step computes the detection statistic at the exact template. If the candidate is due to a signal, the exact template is closer to the signal template and the detection statistic on average increases.

The distribution of the detection statistic $\hat{\beta}_{\rm S/GLtLr}$ and $2\overline{\mathcal{F}}_r$ for these candidates is shown in Figure 2. We use $\hat{\beta}_{\rm S/GLtLr}$ to rank our candidates but also show $2\overline{\mathcal{F}}_r$ because its distribution in Gaussian noise is known. A detectable signal would look like

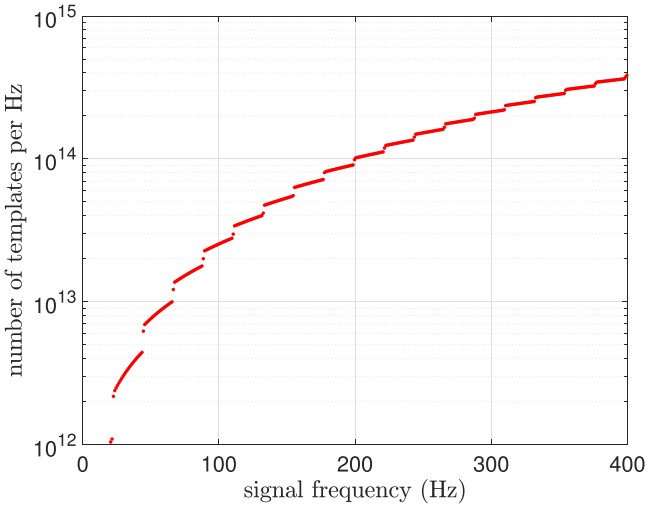

Figure 1. Number of templates searched in 1 Hz bands as a function of signal frequency.

an obvious outlier in both distributions. In Figure 2 we instead see an outlier in the $2\overline{\mathcal{F}}_r$ distribution but not in the $\hat{\beta}_{\rm S/GLtLr}$ distribution. This is an indication that a coherence in one of the two detectors is causing the high value of $2\overline{\mathcal{F}}_r$. In particular the $2\overline{\mathcal{F}}_r$ outlier has a value of 32.9, whereas its $\hat{\beta}_{\rm S/GLtLr} = 2.0$, which is in 5th percentile of lowest values. We follow up this candidate with a semicoherent search with $T_{\rm coh} = 2760$ hr. The most significant result $2\overline{\mathcal{F}}_r = 54.6$ is lower than what one would expect from a signal. The expectation for signals is formed with Monte Carlo simulations of over a thousand fake IT2 signals, added to the O2 data. The data are then processed as in the Einstein@Home search and followed up with the same semicoherent $T_{\rm coh} = 2760$ hr search as used for the candidate. *All* of the signals show an increase in the detection statistic from the Einstein@Home search to the follow-up, larger than what we find for the candidate. We hence conclude that this candidate is not consistent with our signal model. After excluding this candidate, Figures 2 shows no significant signal candidate in either $2\overline{\mathcal{F}}_r$ or $\hat{\beta}_{\rm S/GLtLr}$.

Papa et al. (2020) find a subthreshold candidate at around 369 Hz using the O1 data. This candidate has a $2\mathcal{F} = 57.0$[4] in the fully coherent follow-up search of the first half of O2 data, with a p-value of about 4%. In the presence of an IT2 signal, if the measured $2\mathcal{F}$ is close to the expected value, the $S/N^2 \simeq 57 - 4$. This leads to an expected $2\mathcal{F} \approx 110.0$ and a standard deviation of ≈ 21 in the fully coherent search of the whole O2 data set. A fully coherent search using the whole O2 data set around that candidate falls short of the expectation.

The lowest $2\overline{\mathcal{F}}_r$ value among the candidates followed up in the search presented here is 18.2. It corresponds to a $2\mathcal{F} = 75.0$ in the fully coherent search of the whole O2 data

[4] In a fully coherent search $2\mathcal{F}_r = 2\mathcal{F}$ and, of course, $\overline{\mathcal{F}} = \mathcal{F}$.

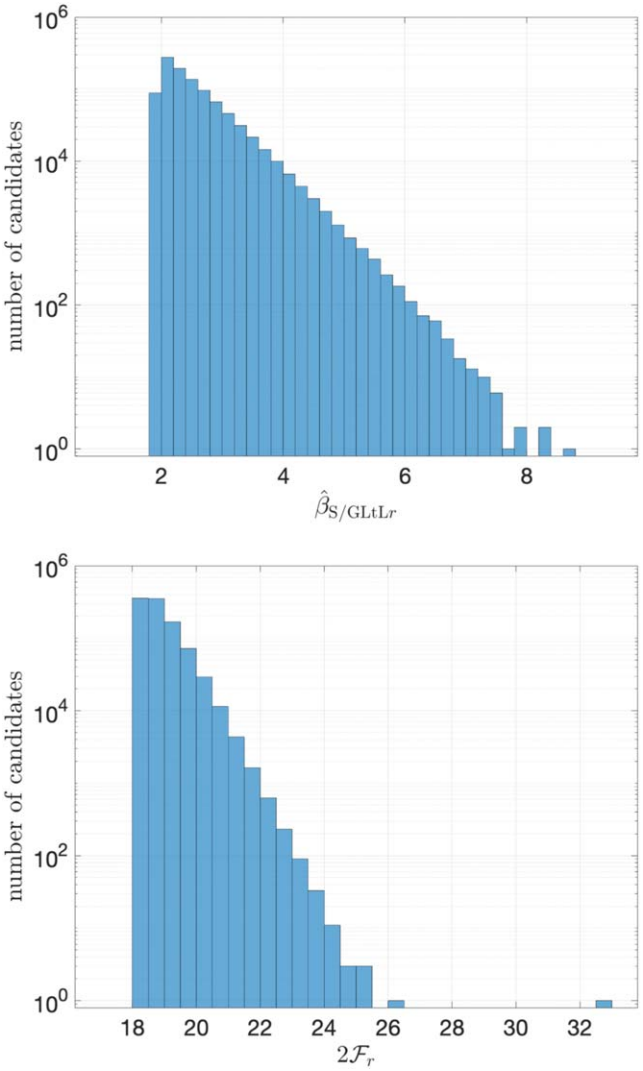

Figure 2. Distribution of the detection statistics $\hat{\beta}_{\mathrm{S/GLtLr}}$ (top) and $2\mathcal{F}_r$ (bottom) of the top 1 million candidates ranked according to $\hat{\beta}_{\mathrm{S/GLtLr}}$, which is the line and transient-line robust statistic.

set. This search is thus not as sensitive to IT2 signals as the fully coherent O2 follow-up that we performed in Papa et al. (2020). It does however cover the entire parameter space of the original O1 search, not just the small volume around the candidate parameters, and it is more sensitive than the original O1 search. In addition, since it is a semicoherent search, it is more robust to deviations of the signal waveform from the assumed model. So, if the original candidate was due to a signal that deviated a bit from the IT2 model, the current search might well produce a candidate whose parameters are close to, although not perfectly consistent with, those of the candidate from the previous search. This would warrant further investigations. The search however does not show any significant candidates that can be associated with that subthreshold O1 candidate.

5.1. Upper Limits

We determine the smallest h_0 that would have produced a detection statistic as high as the most significant measured in every half Hz band. We assume the source to be at the position of our target, the spindown to be in the target range, and the frequency varying in each half Hz. We set the confidence level

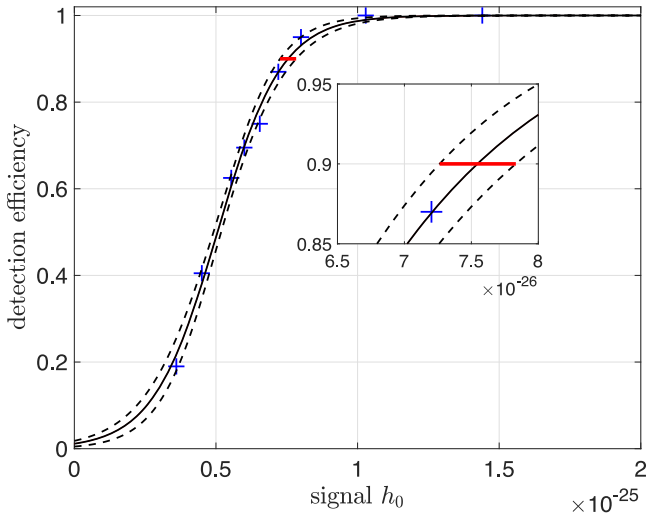

Figure 3. Blue crosses: measured detection efficiency $C(h_0)$ from search-and-recovery Monte Carlos in the frequency band 149–149.5 Hz. The solid line is the best fit and the dashed lines represent 95% confidence intervals on the fit. The red line marks the 90% detection rate, with the uncertainties introduced by this fitting procedure of 4%. The inset shows a zoom around the 90% confidence level.

at 90%, meaning that 90% of the signals in the considered range with an amplitude at the upper-limit value $h_0^{90\%}$ would yield a value of the detection statistic larger than the loudest search result from that parameter range. We use the $\hat{\beta}_{\mathrm{S/GLtLr}}$ as our reference statistic, since it is our ranking statistic.

In each half Hz band, 200 simulated signals with a fixed value of the intrinsic amplitude h_0 are added to the real detector data. The data are then processed as the data that were searched, i.e., they are gated and line-cleaned.

The parameters of simulated signals, the frequency, inclination angle $\cos\iota$, polarization ψ, and initial phase values are uniformly randomly distributed in their respective ranges. The spindown values, $\dot{f}$ and $\ddot{f}$, are log-uniformly randomly distributed in their respective ranges.

A search is performed to recover each injection with the same grid and setup as in the original Einstein@Home search. The search is more limited than the original search to save computations, and covers the parameter space neighboring the fake signal. The fake signal is counted as recovered if the $\hat{\beta}_{\mathrm{S/GLtLr}}$ from the search is higher than the maximum $\hat{\beta}_{\mathrm{S/GLtLr}}$ from the Einstein@Home results in the same half Hz band.

This whole procedure is repeated for various values of h_0. For each value of h_0, the fraction of detected injections is determined in this way and by varying h_0 the confidence $C(h_0)$ curve is constructed. We use a fit with a sigmoid of the form:

$$C(h_0) = \frac{1}{1 + \exp\left(\frac{\mathrm{a} - h_0}{\mathrm{b}}\right)}, \tag{5}$$

and from it we read off the h_0 amplitude that corresponds to 90% confidence, our upper limit value.

The Matlab nonlinear regression prediction confidence intervals routine `nlpredci` is used to yield the best fit for a and b values and the covariance matrix. This covariance matrix can be used to compute the 95% credible interval on the fit of $h_0^{90\%}$. Figure 3 shows the sigmoid curve fitting for the 149 −149.5 Hz band, as a representative example of the results obtained with this procedure. The best fit for $h_0^{90\%}$ in this band

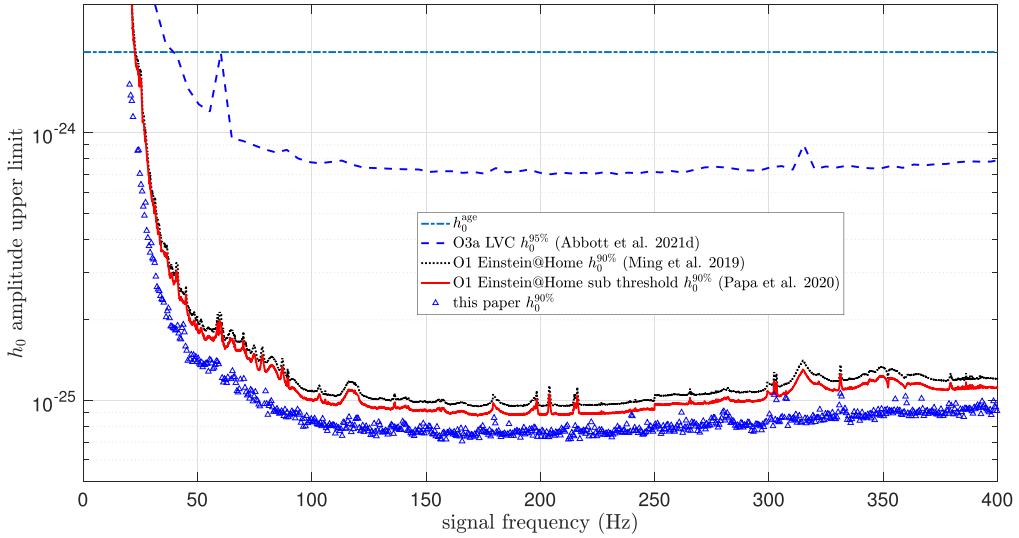

Figure 4. The 90% confidence upper limits on the gravitational wave amplitude of continuous gravitational wave signals from G347.3 for signals with frequencies between 20 and 400 Hz. The lower blue triangles are the results of this search and we compare them with results from previous searches. The blue dots are the upper limits from the LVC search of the O3a (Abbott et al. 2021d); the black dots are Einstein@Home results from O1 data (Ming et al. 2019), and the red solid line is the subthreshold search (Papa et al. 2020).

is 7.5×10^{-26}. The uncertainties introduced by this procedure are less than 4%. The total uncertainty in the upper limit is the sum of the fitting procedure uncertainty and the calibration uncertainties. We conservatively use 5% as the calibration uncertainty (Cahillane et al. 2017).

The $h_0^{90\%}$ upper limits are shown in Figure 4 and are provided in machine readable format at https://www.aei.mpg.de/continuouswaves/O2G347-DirectedSearches.

In nineteen half Hz bands (2.5% of the total) we do not set an upper limit; therefore, in the upper-limit files we have 741 entries rather than 760. The cleaning procedure substitutes disturbed frequency-domain data with Gaussian noise in order to avoid further spectral contamination from "leakage" in the search results. Those bands are consistently cleaned in the upper-limit Monte Carlos after a signal is injected, so it may happen that most of the injected signal is removed. When that happens, no matter how loud the signal is, the detection efficiency does not increase. In these bands the 90% detection rate level cannot be reached and we do not set any upper limit. This reflects the fact that, even if we had a signal there, because of the cleaning procedure, we could not detect it. In the nineteen half Hz bands where the 90% confidence level is not reached, 25% of the data had on average been cleaned away.

In other bands the cleaning procedure partly or completely removes some of the signals, depending on their frequency. So, in order to produce a detection statistic value above a given threshold, statistically, a louder signal is required than in nearby bands that are not cleaned. In those bands the upper limit is higher than what it would be if the data had not been cleaned. For example, $h_0^{90\%}$ of the band 331–331.5 Hz is about 15% larger than the $h_0^{90\%}$ of the neighboring half Hz bands. In this band, 8% of the data are Gaussian noise data.

5.2. Upper Limits on the Astrophysical Parameters

The h_0 upper limits can be converted to constraints on the equatorial ellipticity ε of the neutron star at distance D and at frequency f (Zimmermann & Szedenits 1979):

$$\varepsilon = \frac{c^4}{4\pi^2 G}\frac{h_0 D}{I f^2}, \tag{6}$$

where c is the speed of light, G is the gravitational constant, and I the principal moment of inertia of the star. Assuming a fiducial value of the principal moment of inertia of 10^{38} kg m^2 and $D = 1.3$ kpc, we convert $h_0^{90\%}(f)$ into upper limits on the ellipticity of the source G347.3. These are shown in Figure 5.

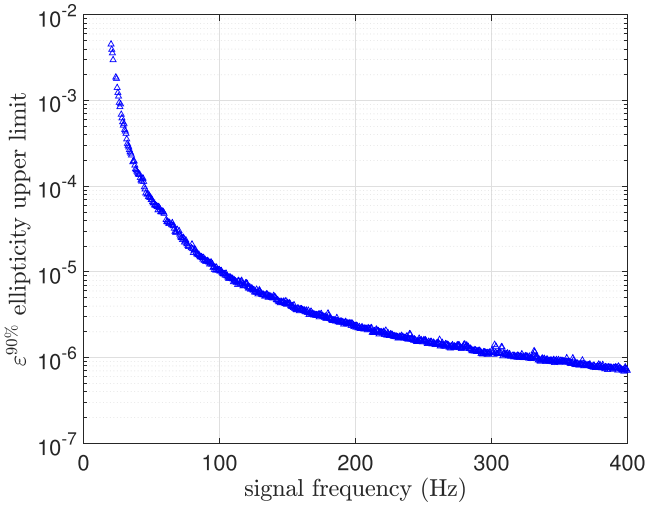

Figure 5. Upper limits on the equatorial ellipticity of G347.3. We assume a distance of 1.3 kpc.

R-mode oscillations of a spinning neutron star also produce continuous gravitational waves. The amplitude h_0 for a signal with frequency f from a source at a distance D depends on the r-mode amplitude α as follows (Owen 2010):

$$\alpha = 0.028\left(\frac{h_0}{10^{-24}}\right)\left(\frac{D}{1\ \text{kpc}}\right)\left(\frac{100\ \text{Hz}}{f}\right)^3. \tag{7}$$

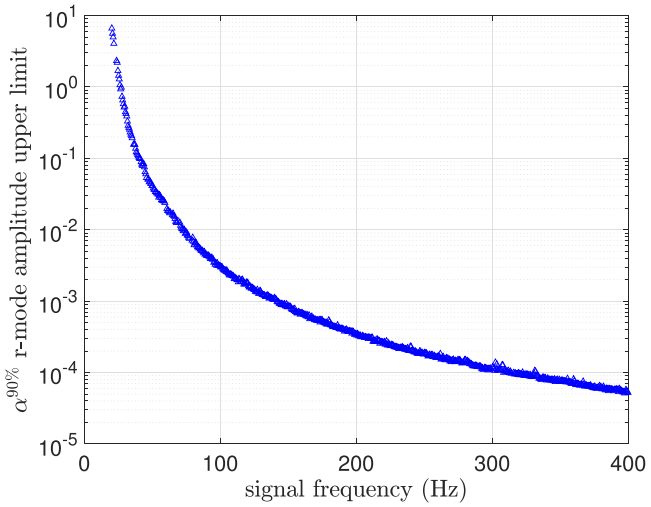

Figure 6. Upper limits on the *r*-mode amplitude.

Our $h_0^{90\%}$ upper limits can then be recast as upper limits on the *r*-mode amplitude. The result is shown in Figure 6.

6. Conclusions

In this paper we present results from the most sensitive search to date for continuous gravitational wave emission from the SNR G347.3-0.5 in the frequency range 20−400 Hz and the broadest first and second frequency-derivative ranges. Electromagnetic pulsations have not been detected from this object, and the direct observation of continuous gravitational emission would provide the first gravitational wave pulsar timing solution.

We prioritize this target with respect to other SNRs because of a subthreshold candidate from a previous search. We do not find a signal. Our findings are consistent with those of Tenorio et al. (2021).

We constrain the amplitude of continuous gravitational wave emission at a level that is more than a factor of 20 smaller than the indirect age-based limit over most of the frequency range. The most constraining intrinsic gravitational wave amplitude upper limit is 7.0×10^{-26} near 166 Hz. This result improves over our O1 result (Ming et al. 2019) and over the extensive subthreshold O1 search (Papa et al. 2020). It is also more constraining than the recent search result of Abbott et al. (2021d) that uses the significantly more sensitive O3a data. In fairness, we note however that Abbott et al. (2021d) search a broader frequency range and their search uses a technique that is more robust to possible deviations of the signal from the IT-*n* model.

Recast in terms of equatorial ellipticity of the neutron star, our results constrain it to be below 10^{-6} at frequencies higher than ≈320 Hz, reaching bounds of 6.9×10^{-7} at 400 Hz. This is a physically plausible value of neutron star deformation (Johnson-McDaniel & Owen 2013; Gittins et al. 2020; Gittins & Andersson 2021). Such a limit is not matched in Abbott et al. (2021d) even at 2000 Hz.

Our spindown range is high enough to allow for braking indexes as high as 7, encompassing *r*-mode emission. Our null result can then constrain the *r*-mode amplitude and does so at a level below 10^{-4} at frequencies higher than ≈310 Hz. This is also a physically possible value (Haskell 2015).

This is the first O2 public data Einstein@Home search for continuous gravitational waves from SNRs and probes a physically interesting range of source parameters. Building on this, future searches will extend the parameters space and/or include more targets and/or more data, pushing further into interesting territory.

We gratefully acknowledge the support of the many thousands of Einstein@Home volunteers who made this search possible.

We acknowledge support from the Max Planck Society for Projects QPQ10003 and QPQ10004, and the NSF grant No. 1816904.

A lot of post-processing is run on the ATLAS cluster at AEI Hannover. We thank Carsten Aulbert and Henning Fehrmann for their support.

We would like to thank the instrument scientists and engineers of LIGO whose amazing work has produced detectors capable of probing gravitational waves so incredibly small.

This research has made use of data, software, and/or web tools obtained from the Gravitational Wave Open Science Center (https://www.gw-openscience.org/), a service of LIGO Laboratory, the LIGO Scientific Collaboration and the Virgo Collaboration. LIGO Laboratory and Advanced LIGO are funded by the United States National Science Foundation (NSF) as well as the Science and Technology Facilities Council (STFC) of the United Kingdom, the Max-Planck-Society (MPS), and the State of Niedersachsen/Germany for support of the construction of Advanced LIGO and construction and operation of the GEO600 detector. Additional support for Advanced LIGO was provided by the Australian Research Council. Virgo is funded, through the European Gravitational Observatory (EGO), by the French Centre National de Recherche Scientifique (CNRS), the Italian Istituto Nazionale di Fisica Nucleare (INFN) and the Dutch Nikhef, with contributions by institutions from Belgium, Germany, Greece, Hungary, Ireland, Japan, Monaco, Poland, Portugal, and Spain.

ORCID iDs

J. Ming https://orcid.org/0000-0002-2150-3235
M. A. Papa https://orcid.org/0000-0002-1007-5298
H.-B. Eggenstein https://orcid.org/0000-0001-5296-7035

References

Aasi, J., Abbott, B. P., Abbott, R., et al. 2015, CQGra, 32, 074001
Abbott, B. P., Abbott, R., Abbott, T. D., et al. 2019a, ApJ, 879, 10
Abbott, B. P., Abbott, R., Abbott, T. D., et al. 2019b, PhRvD, 100, 024004
Abbott, B. P., Abbott, R., Abbott, T. D., et al. 2019c, ApJ, 875, 122
Abbott, R., Abbott, T. D., Abraham, S., et al. 2021a, ApJL, 913, L27
Abbott, R., Abbott, T. D., Abraham, S., et al. 2021b, PhRvD, 103, 064017
Abbott, R., Abbott, T. D., Abraham, S., et al. 2021c, PhRvD, 104, 082004
Abbott, R., Abbott, T. D., Abraham, S., et al. 2021d, ApJ, 921, 80
Abbott, R., Abbott, T. D., Abraham, S., et al. 2021e, ApJ, 922, 71
Abbott, R., Abbott, T. D., Abraham, S., et al. 2021f, SoftX, 13, 100658
Allen, B., & Mendell, G. 2004, https://dcc.ligo.org/LIGO-T040164/public
Anderson, D. P. 2004, in Proc. Fifth IEEE/ACM Int. Workshop on Grid Computing (GRID04), 4
Anderson, D. P., Christensen, C., & Allen, B. 2006, in Proc. 2006 ACM/IEEE Conf. on Supercomputing, 126
Ashok, A., Beheshtipour, B., Papa, M. A., et al. 2021, ApJ, 923, 85
Beheshtipour, B., & Papa, M. A. 2020, PhRvD, 101, 064009
Beheshtipour, B., & Papa, M. A. 2021, PhRvD, 103, 064027
Cahillane, C., Betzwieser, J., Brown, D. A., et al. 2017, PhRvD, 96, 102001
Cassam-Chenaï, G., Decourchelle, A., Ballet, J., et al. 2004, A&A, 427, 199

Covas, P. B., & Sintes, A. M. 2020, PhRvL, 124, 191102
Covas, P. B., Effler, A., Goetz, E., et al. 2018, PhRvD, 97, 082002
Cutler, C., & Schutz, B. F. 2005, PhRvD, 72, 063006
Davis, D., Massinger, T., Lundgren, A., et al. 2019, CQGra, 36, 055011
Dergachev, V., & Papa, M. A. 2020, PhRvL, 125, 171101
Dergachev, V., & Papa, M. A. 2021a, PhRvD, 104, 043003
Dergachev, V., & Papa, M. A. 2021b, PhRvD, 103, 063019
Dergachev, V., Papa, M. A., Steltner, B., & Eggenstein, H.-B. 2019, PhRvD, 99, 084048
Einstein@Home 2019, The Volunteer Computing Project Einstein@Home, https://einsteinathome.org/
Fesen, R. A., Kremer, R., Patnaude, D., & Milisavljevic, D. 2012, AJ, 143, 27
Fesik, L., & Papa, M. A. 2020, ApJ, 895, 11
Gittins, F., & Andersson, N. 2021, MNRAS, 507, 116
Gittins, F., Andersson, N., & Jones, D. I. 2020, MNRAS, 500, 5570
Haskell, B. 2015, IJMPE, 24, 1541007
Jaranowski, P., Krolak, A., & Schutz, B. F. 1998, PhRvD, 58, 063001
Johnson-McDaniel, N. K., & Owen, B. J. 2013, PhRvD, 88, 044004
Keitel, D. 2016, PhRvD, 93, 084024
Keitel, D., Prix, R., Papa, M. A., Leaci, P., & Siddiqi, M. 2014, PhRvD, 89, 064023
Lasky, P. D. 2015, PASA, 32, e034
LIGO 2019, The O2 Data Release, doi:10.7935/CA75-FM95
Lindblom, L., & Owen, B. J. 2020, PhRvD, 101, 083023
Mignani, R. P., Zaggia, S., de Luca, A., et al. 2008, A&A, 484, 457
Millhouse, M., Strang, L., & Melatos, A. 2020, PhRvD, 102, 083025
Ming, J., Krishnan, B., Papa, M. A., Aulbert, C., & Fehrmann, H. 2016, PhRvD, 93, 064011
Ming, J., Papa, M. A., Singh, A., et al. 2019, PhRvD, 100, 024063
Owen, B. J. 2010, PhRvD, 82, 104002
Owen, B. J., Lindblom, L., Cutler, C., et al. 1998, PhRvD, 58, 084020
Papa, M. A., Ming, J., Gotthelf, E. V., et al. 2020, ApJ, 897, 22
Piccinni, O. J., Astone, P., D'Antonio, S., et al. 2020, PhRvD, 101, 082004
Pletsch, H. J. 2008, PhRvD, 78, 102005
Pletsch, H. J. 2010, PhRvD, 82, 042002
Pletsch, H. J., & Allen, B. 2009, PhRvL, 103, 181102
Singh, A., Papa, M. A., Eggenstein, H.-B., & Walsh, S. 2017, PhRvD, 96, 082003
Steltner, B., Papa, M. A., & Eggenstein, H.-B. 2021a, arXiv:2105.09933
Steltner, B., Papa, M. A., Eggenstein, H.-B., et al. 2021b, ApJ, 909, 79
Tenorio, R., Keitel, D., & Sintes, A. M. 2021, PhRvD, 104, 084012
Wang, Z. R., Qu, Q. Y., & Chen, Y. 1997, A&A, 318, L59
Wette, K., Owen, B. J., Allen, B., et al. 2008, CQGra, 25, 235011
Zhang, Y., Papa, M. A., Krishnan, B., & Watts, A. L. 2021, ApJL, 906, L14
Zhu, S. J., Papa, M. A., Eggenstein, H.-B., et al. 2016, PhRvD, 94, 082008
Zimmermann, M., & Szedenits, E. 1979, PhRvD, 20, 351